Available online at www.sciencedirect.com
SCIENCE DIRECT®
ELSEVIER
Earth and Planetary Science Letters 218 (2004) 521–537
EPSL
www.elsevier.com/locate/epsl

Kinetics of bubble nucleation in a rhyolitic melt: an experimental study of the effect of ascent rate

Catherine C. Mourtada-Bonnefoi, Didier Laporte *

Laboratoire Magmas et Volcans, CNRS et Université Blaise Pascal, OPGC, 5 rue Kessler, 63038 Clermont-Ferrand Cedex, France

Received 19 June 2003; received in revised form 10 November 2003; accepted 20 November 2003

Abstract

In order to characterize the effect of ascent rate on the kinetics of bubble nucleation in a rhyolitic magma, we performed three series of experiments decompressed at rates of either 1000, 167, or 27.8 kPa/s. The experiments were carried out in an externally heated pressure vessel at 800°C and in the pressure range 260–59 MPa; the starting material was a crystal-free and bubble-free rhyolitic glass containing 7.0 wt% dissolved H_2O. In all the decompression experiments, homogeneous bubble nucleation began at 90 ± 2 MPa, that is, $\approx$150 MPa below the water saturation pressure of the silicate liquid, 240 MPa. The degree of supersaturation ΔP_{HoN} required to trigger homogeneous bubble nucleation was almost independent of decompression rate (ΔP_{HoN} is the difference between the saturation pressure and the nucleation pressure): nucleation pressure decreased by ≤ 3 MPa for a 36-fold increase in decompression rate. These results are in good agreement with the classical theory of nucleation assuming a rhyolite–H_2O surface tension of 0.106 N m^{-1}. Our major experimental finding is that, after a short nucleation event, the nucleation rate dropped and the bubble number density N reached a stationary value that was strongly sensitive to decompression rate: 6.8 mm^{-3} at 27.8 kPa/s, 470 mm^{-3} at 167 kPa/s, and 5800 mm^{-3} at 1000 kPa/s. The smaller value of N at low decompression rate was compensated by a larger mean bubble size, so that, at a given pressure, vesicularity was almost independent of decompression rate. The experimental values of N can be reproduced within a factor 0.3–1.4 using a relationship derived from published numerical simulations of vesiculation in ascending magmas. The nucleation behavior in our experiments is dictated by a competition between bubble nucleation and diffusive bubble growth, which depletes in water the surrounding liquid and therefore reduces the degree of volatile supersaturation. Once a critical value of N is attained, diffusive bubble growth can keep pace with decompression and prevent the degree of volatile supersaturation in the liquid to increase with decreasing pressure. The strong correlation between bubble number density and decompression rate has fundamental volcanological implications. If we extrapolate the experimental data to the typical ascent rates of silicic magmas, we obtain bubble number densities (10^{-3}–10^{1} mm^{-3} for homogeneous nucleation; $\approx 10^{-1}$–10^{3} mm^{-3} for heterogeneous nucleation) that are orders of magnitude smaller than those measured in most natural pumices. We therefore propose that the large values of N in silicic pumices may be due to two successive nucleation events: (1) a first event, which occurs relatively deep in the volcanic conduit and which yields a moderate number of bubbles; and (2) a second nucleation event, yielding a very large number of small bubbles, and presumably related to the dramatic increase of decompression rate that precedes fragmentation. The small bubble number densities associated with homogeneous nucleation suggest that a strong departure from

* Corresponding author. Tel.: +33-4 7334 6733; Fax: +33-4 7334 6744.
E-mail address: laporte@opgc.univ-bpclermont.fr (D. Laporte).

0012-821X/03/$ – see front matter
doi:10.1016/S0012-821X(03)00684-8

equilibrium degassing should be the rule even at slow ascent rates.

Keywords: magmas; nucleation; bubbles; decompression; degassing

1. Introduction

Explosive volcanic eruptions are powered by the rapid exsolution of volatile components (mainly H_2O) initially dissolved in the magma. The rate of volatile exsolution and vesiculation (bubble nucleation and growth) in volcanic conduits controls the dynamics of magma ascent and eruption [1–6]: violent degassing results in explosive activity, whereas slow degassing leads to the extrusion of lava domes and flows. A major aspect of the vesiculation process is the kinetics of bubble nucleation, which controls two fundamental parameters: the critical nucleation pressure and the number density of bubbles [4,7]. The critical pressure of bubble nucleation is the pressure at which bubbles begin to nucleate. Due to the relatively large interfacial energy between a H_2O-rich bubble and a silicic liquid (of the order of 0.1 J m^{-2}), the difference between the volatile saturation pressure of the liquid and the nucleation pressure may be very large (in excess of 100 MPa in the case of homogeneous nucleation [8–10]), resulting in strongly delayed nucleation during magma ascent and in the build-up of very large degrees of volatile supersaturation. The number density of bubbles is also a crucial parameter because it determines the length scale of diffusion of volatile molecules, and therefore the evolution of the volume fraction of bubbles and of the degree of volatile supersaturation during magma ascent. In particular, if the number of bubbles per unit volume is large, decompression can result in extreme rates of magma expansion and acceleration [1].

Despite recent experimental studies of decompression-induced vesiculation in ascending magmas [8–15], many aspects of bubble nucleation remain poorly constrained, such as the effect of decompression rate on nucleation kinetics, or the effect of volatile composition or silicate liquid composition on nucleation pressures. This study is devoted to the effect of decompression rate on the kinetics of homogeneous bubble nucleation in a rhyolitic liquid containing 7 wt% water, at 800°C. To simulate reproducibly the ascent of a magma, we designed a decompression system [16], allowing us to decrease automatically the pressure in an externally heated pressure vessel by steps of 0.1–1 MPa, at a rate of ≤ 0.3 kPa/s to 200 kPa/s (Fig. 1). For comparison, ascent rates of silicic to intermediate magmas range from 1 mm/s to 10 m/s and correspond to decompression rates of 0.025 kPa/s to 250 kPa/s [17]. The decompression device comprises a series of computer-controlled valves that automatically take up small volumes ΔV of pressurizing gas (nitrogen) from the autoclave; each gas intake produces a very small decrease in pressure, ΔP, because ΔV is three to four orders of magnitude smaller than the autoclave volume (25 cm^3). Volumes ΔV were chosen to produce pressure drops of 0.1–1 MPa along the whole decompression path: ΔV was equal to 0.01 cm^3 at $P = 200$ MPa and increased with decreasing pressure (for instance, $\Delta V \approx 0.05$ cm^3 at $P = 50$ MPa). The time lapse between a pressure drop ΔP and the next pressure drop was automatically adjusted to yield the decompression rate set by the operator. Our decompression system will be described in detail in a following paper.

Two series of automatic decompression experiments were performed at linear rates of 167 and 27.8 kPa/s (600 and 100 MPa per hour, respectively). In addition, a third series of manual decompression experiments at 1000 kPa/s was made to enlarge the range of decompression rates. Major textural changes were observed as a function of decompression rate. The experimental results and the main volcanological implications are summarized in this paper.

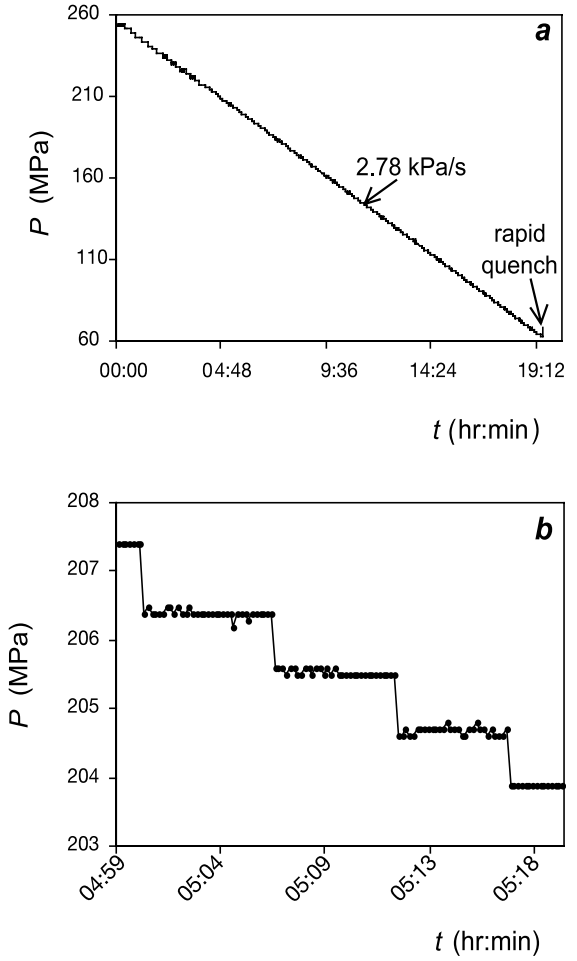

Fig. 1. (a), (b) An illustration of the performance of the automatic decompression device. (a) Plot of pressure as a function of time in an experiment with a decompression rate of 2.78 kPa/s, an initial pressure of 253 MPa, and a quench pressure of 68.3 MPa. The height of the first decompression steps is $\Delta P \approx 2.5$ MPa, but ΔP rapidly decreases with decreasing pressure: below 215 MPa, ΔP is always ≤ 1.0 MPa. (b) Detail of the decompression path showing four pressure drops ($\Delta P \approx 0.9$ MPa) between $P = 207.4$ MPa and $P = 203.9$ MPa.

2. Experimental and analytical techniques

2.1. Starting glasses

The starting material was a rhyolitic obsidian from Güney Dagi, Turkey (76.51% SiO_2, 12.56% Al_2O_3, 0.70% FeO, 0.01% MgO, 0.25% CaO, 4.47% Na_2O, 4.24% K_2O, 0.03% TiO_2, 0.07% MnO [9]). Obsidian cylinders 2.5 mm in diameter were saturated in water at 250 MPa and 1000°C to produce bubble- and crystal-free rhyolitic glasses containing ≈ 7 wt% H_2O (Table 1). The cylinders were loaded into platinum capsules along with 10 wt% tridistilled H_2O. After welding, the capsules were loaded into outer platinum containers along with a Ni–NiO mixture and distilled water to buffer the oxygen fugacity. The saturation experiments were made in an internally heated pressure vessel, and were terminated by isobaric quench. Pressure was measured with a manganine gauge and controlled within ± 1 MPa; the difference between the reading of the manganine gauge and the reading of a calibrated bourdon tube was ≤ 2 MPa (at 250 MPa).

At the end of the saturation experiments, the inner capsules were weighed, then pierced with a needle and stored in an oven at 130°C to measure the mass of free water left. The glass cylinders were carefully removed from the platinum capsules: they were all bubble-free and colorless to slightly grayish. Electron probe microanalysis indicated that $\approx 40\%$ of the iron oxide in the starting obsidian was lost to the platinum capsule during the saturation experiments. The glasses were cut in two parts: a long part, about 3 mm long, that was kept for a decompression experiment; and a short part that was put aside for Fourier transform infrared (FTIR) spectroscopy.

2.2. Decompression experiments

The starting glass was welded in a platinum capsule (with no free water added). The capsule was placed in an externally heated pressure vessel fitted with a rapid quench extension. It was first cold-pressurized to 230–240 MPa and then heated to 800°C in 60–90 min. During heating, pressure increased and reached the target value, 260 MPa, at ≤ 400°C; then pressure was kept within +10/−5 MPa of 260 MPa until the end of the heating stage. We used nitrogen gas as the pressure medium; pressure was measured by a pressure transducer accurate to 1 MPa (in the P range of interest). Oxygen fugacity was not buffered during the decompression experiments, but was assumed to

Table 1
Decompression experiments: a summary of run information[a]

Run no.	H_2O[b] (wt%)	$-dP/dt$[c] (kPa/s)	P_f[c] MPa	N_{bubble}[d]	D[e] (μm)	D_{2D}[e] (μm)	V[f] (vol%)	N[g] (mm^{-3})	Final H_2O[h] (wt%)
C22	n.d.	27.8	92.1	0	0	0	0	0	n.d.
C20	n.d.	27.8	88.6	8	77.3 (45.4)	n.d.	0.3	6.7	6.81 (52)
C19	7.04	27.8	85.1	3	186.7 (27.2)	n.d.	2.9	8.4	n.d.
C8	6.83	27.8	79.5	10	257.5 (20.3)	n.d.	5.7	6.6	6.16 (31)
C11	7.00	27.8	70.4	2	377.9 (8.2)	n.d.	13.2	5.4	6.89 (41)
B21	n.d.	167	90.5	0	0	0	0	0	n.d.
B18	7.04	167	84.4	23	41.1 (13.1)	n.d.	0.3	75	6.64 (39)
B15	6.86	167	80.2	10 [131]	59.5	54.7 (12.1)	5.1	580 [160]	6.92 (42)
B14	7.05	167	70.7	30 [112]	76.6	67.1 (14.3)	12.8	350 [300]	6.51 (70)
B23	n.d.	167	59.3	128	101.9	99.4 (38.0)	31.9	480	4.80 (83)
A3	7.01	980	118.9	0	0	0	0	0	n.d.
A4	6.92	1000	98.9	0	0	0	0	0	6.94 (35)
A5	6.94	1030	88.4	2	18.8 (1.3)	n.d.	0.0	4.0	6.48 (19)
A6	6.94	1240	85.0	44 [291]	18.9	18.4 (4.7)	1.5	2300 [2100]	6.96 (35)
A2	6.92	960	79.2	106 [466]	23.1	22.7 (8.2)	2.6	2300 [2300]	7.32 (24)
A13	7.04	1240	69.6	287	32.7	30.2 (8.3)	17.6	7600	6.26 (53)
A1	7.02	820	58.9	231	54.1	48.0 (12.7)	31.2	4100	5.08 (61)

[a] The textural parameters in the table correspond exclusively to homogeneous nucleation textures in the core of the samples.
[b] Water content in the starting glasses, measured by FTIR spectroscopy (n.d.: not determined). Most starting glasses were 2.5 mm in diameter except those used in runs C19 and B18 (3.3 mm in diameter). They were saturated with water in an internally heated pressure vessel at 250 MPa and 1000°C, for durations of 48–54 h (except for runs C19 and B18: 142 h).
[c] $-dP/dt$ is the decompression rate and P_f is the pressure at which the experiment was quenched.
[d] N_{bubble} is the number of bubbles used in the quantitative treatment. In glasses containing a few bubbles (C20, C19, C8, C11, B18, A5), all the bubbles in the vesiculated core were counted and measured in thick sections by optical microscopy. In the case of bubble-rich samples (B15, B14, B23, A6, A2, A13, A1), N_{bubble} is the number of bubbles analyzed in a polished section with the scanning electron microscope. For comparison, the number densities of bubbles in B15, B14, A6 and A2 were also measured in thick sections by optical microscopy (numbers in brackets in columns 'N_{bubble}' and 'N').
[e] Mean diameter of bubbles, D. In bubble-rich samples, we first measured the mean bubble size in a polished section, D_{2D}, and the 2D BSDs (bubbles were assumed to be spherical); the 3D distributions were then derived from the 2D distributions using the Schwartz–Saltykov method and were used to compute the 3D mean bubble diameter, D, and the bubble number density, N (the 1σ standard deviation is given in parentheses).
[f] Vesicularity V. In the case of thick sections, V is equal to the total volume of bubbles divided by the volume of the vesiculated core. In the case of polished sections, the 3D vesicularity is assumed to be equal to the 2D vesicularity measured in the polished sections.
[g] The number density of bubbles, N, is defined as the number of bubbles per unit volume of glass.
[h] The mean water content of glasses in bubble-free regions at the end of the decompression experiments was derived from electron probe microanalyses by attributing to H_2O the difference between 100% and the analytical total (the 1σ standard deviation, in parentheses, is given in terms of the least unit cited). We used a Cameca SX 100 electron probe with the following analytical conditions: 15 kV, 8 nA, counting times of 10 s, and a defocussed beam 10 μm in diameter. All glasses were analyzed in a single microprobe session for internal consistency.

remain close to the Ni–NiO buffer (as in the saturation experiments) because of the short run durations involved. All experiments began by a 15-min relaxation stage at 260 MPa, 800°C. Pressure was then decreased to a value P_f, at a rate equal to 27.8, 167, or 1000 kPa/s. As soon as pressure P_f was reached, the experiment was quenched isobarically at an initial rate of 200°C/s. Each experimental series consists in a suite of five to seven experiments quenched at different pressures along the decompression path (Fig. 2; Table 1).

Decompression was performed by two distinct procedures, depending on decompression rate. In the series at 1000 kPa/s, gas pressure was released by carefully opening a valve on the pressure line. In the two other series, decompression was divid-

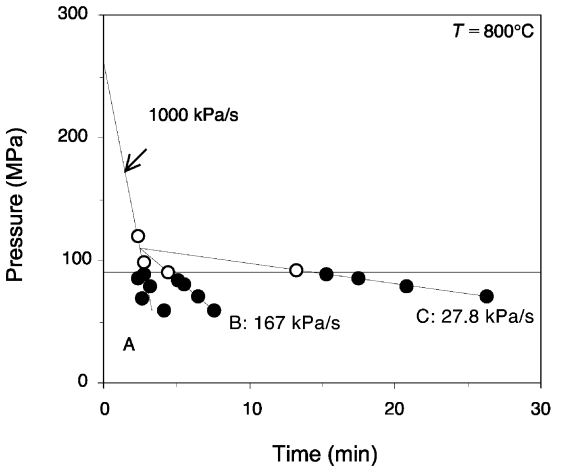

Fig. 2. The nucleation behavior of a rhyolitic liquid with 7 wt% dissolved H_2O was studied at three different decompression rates: 1000, 167, and 27.8 kPa/s (series A, B, and C, respectively). In the 167 and 27.8 kPa/s series, decompression was divided in two steps: pressure was first decreased manually from 260 MPa down to 110 MPa, at a linear rate of 1000 kPa/s; then, it was decreased at 167 kPa/s (series B) or 27.8 kPa/s (series C) to the target value P_f using the automatic decompression device. For each decompression path (thin lines), the experiments were quenched at different pressures P_f shown by the circles: empty and full circles correspond, respectively, to experiments quenched above and below the critical pressure of homogeneous bubble nucleation ($\approx$90 MPa; thin horizontal line).

ed into two steps (Fig. 2). First, pressure was decreased manually from 260 MPa down to 110 MPa, at a rate of 1000 kPa/s. Then we used the automatic decompression device to slowly decrease the pressure to the target value at either 167 or 27.8 kPa/s. The two-step procedure allowed us to reduce significantly the duration of the experiments without affecting the kinetics of bubble nucleation (because nucleation pressures in our study are $<$110 MPa; see below). The motivation was not to save time, but to minimize the water loss from the glass cylinder. In the decompression experiments, before the event of homogeneous nucleation, water tends to diffuse out of the rhyolite cylinders, leading to the formation of a H_2O-depleted rim [9,10]. The main advantage of the two-step decompression procedure is to reduce the time available for dehydration so that the final thickness of the H_2O-depleted rim is small compared with the sample diameter.

2.3. Analytical techniques

2.3.1. FTIR spectroscopy

The water content of most starting glasses was measured by FTIR spectroscopy in doubly polished sections, typically 500 μm thick. We used a Nicolet Magma-IR 760 spectrometer coupled with a Nicolet Nic-Plan microscope at the Institut des Sciences de la Terre d'Orléans, France. The spectrometer operated from 9000 to 2100 cm^{-1} with a resolution of 4 cm^{-1}, using a Globar light source, a CaF_2 beamsplitter, an MCT detector, the signal being averaged over 64 scans. Using the Beer–Lambert law, molecular H_2O and OH^- were derived from the height of the absorbance peaks at 5200 and 4500 cm^{-1}, using molar absorptivities of 1.61 and 1.73 l/mol/cm, respectively [18]. The density of the glasses was computed from the composition of Güney Dagi obsidian following the method of Lange and Carmichael [19]; to take in account the effect of water on density, we used a value of 12 cm^3/mol for the molar volume of water in rhyolitic glasses [20].

FTIR spectroscopy yielded consistent results: water contents in the core of the starting glasses lie between 6.83 and 7.05 wt% (Table 1). If real, this 0.2 wt% variation in H_2O concentration would correspond to a 15 MPa variation in saturation pressure [21,22]. We emphasize, however, that it is mostly due to analytical uncertainty (not better than $\pm$0.1 wt% because the thickness of the doubly polished sections was measured to only $\pm$5 μm). For instance, the water contents analyzed in glasses B14 and B15, which were synthesized in the same saturation experiment and, therefore, must have the same saturation pressure, differ by $\approx$0.2 wt%: 7.05 and 6.86 wt%, respectively. From the uncertainty on pressure measurement and control during the saturation experiments, we estimate that the water saturation pressures of our starting glasses are equal within $\pm$2 MPa.

We stress that the water saturation pressure in the decompression experiments at 800°C is slightly lower than 250 MPa – the pressure of the saturation experiments at 1000°C – because of a slight increase in water solubility with decreasing temperature. Depending on the solubility

model taken in consideration, the 200°C decrease in temperature would correspond to a decrease of the water saturation pressure of 8–9 MPa [22] to 15 MPa [21]. In the following, we consider that the water saturation pressure in the decompression experiments is equal to 240 MPa, with an uncertainty of ±5 MPa.

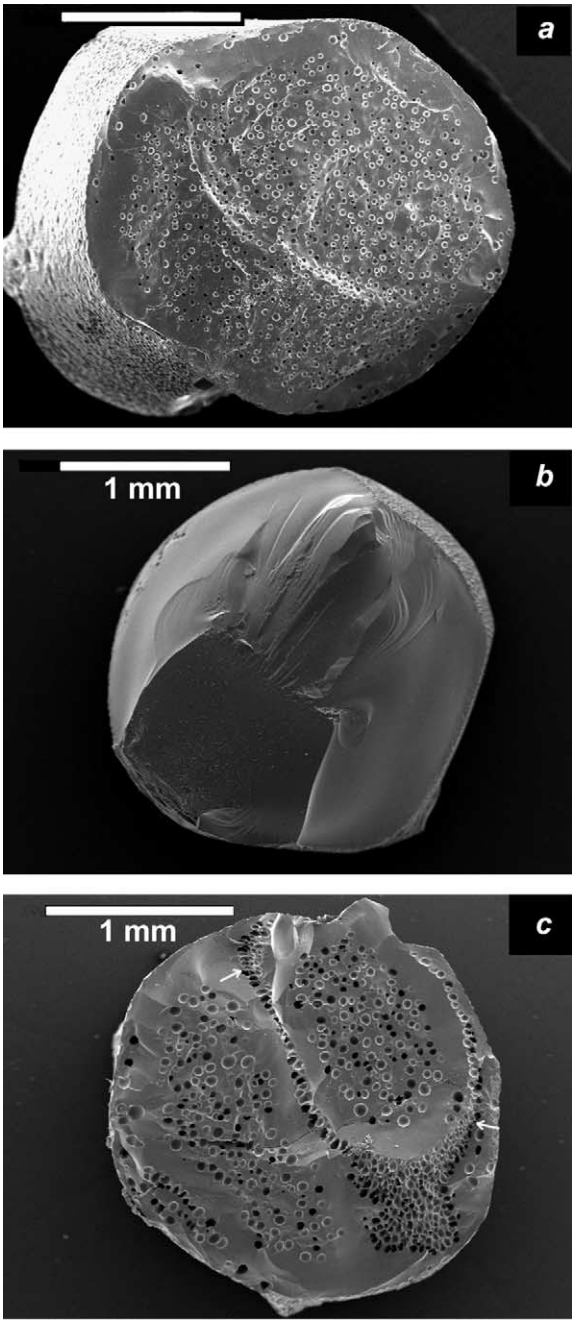

2.3.2. Textural analysis

For samples containing few bubbles, the textural parameters were measured directly under an optical microscope using doubly polished sections ≈1 mm thick. Samples containing numerous bubbles were characterized with a Cambridge Stereoscan S360 scanning electron microscope: nucleation parameters were extracted from microphotographs of polished sections using the NIH image software. The two-dimensional (2D) bubble size distribution (BSD) was derived assuming that bubbles were all spherical; the 3D BSD was computed from the 2D BSD using the Schwartz–Saltykov method [23].

3. Experimental results

3.1. Internal textures of the samples: homogeneous versus heterogeneous nucleation

The interpretation of the experimental series is based exclusively on textures observed in the core of the samples. Sample rims are indeed the place of a number of parasitical phenomena: heterogeneous nucleation of bubbles on the inner wall of the platinum capsule and chemical interactions between the glass cylinder and the air trapped in

←

Fig. 3. (a–c) Scanning electron microscopy microphotographs of fracture surfaces illustrating the internal structures of the samples. (a) Typical structure of a sample quenched at a pressure below the critical pressure of homogeneous bubble nucleation (sample A13: 1000 kPa/s, $P_f = 69.6$ MPa): it shows a densely vesiculated core with a homogeneous texture and a rim, ≈200 μm thick, which contains only a few scattered bubbles; note also, on the left, the bubbly outer surface of the glass cylinder (resulting from heterogeneous nucleation of bubbles on the platinum capsule). (b) Internal structure of a sample quenched at a pressure above the critical pressure of homogeneous bubble nucleation (sample A3: 1000 kPa/s, $P_f = 118.9$ MPa): the sample core is bubble-free (the bright spots in the lower left are glass shards). (c) Sample A1 (1000 kPa/s, $P_f = 58.9$ MPa) showing a vesiculation texture disturbed by a curved bubbly fracture (white arrows). Scale bars: 1 mm.

the capsule. As a result, a glass cylinder at the end of a decompression experiment is composed of two distinct zones (Fig. 3a): a thin rim, typically 200 μm thick, comprising a bubbly outer surface and a glassy layer depleted in water compared to the sample core; and a core, which is either bubble-free or homogeneously vesiculated depending on whether the experiment was quenched above or below the critical pressure of homogeneous bubble nucleation (Fig. 3b and a, respectively). This simple zonation was often disturbed by dense concentrations of bubbles lying along sub-planar or curved surfaces (Figs. 3c and 4a): these 'bubbly fractures' are presumably related to fractures that developed in the glass cylinders at the beginning of the decompression experiments (see [9] for more details).

Basically, our study is founded on the quantification of core textures. The main argument that allows us to conclude that core textures result from an event of homogeneous nucleation is robust: there are no crystals to serve as sites for nucleation, either in the starting glasses or in the final products at the end of the decompression experiments (the absence of crystals was checked by optical and scanning electron microscopy). The absence of crystals in the starting glasses is due to the high temperature of the saturation experiments: 1000°C. The absence of crystals at the end of the decompression experiments is well visible in Fig. 4 and is due to the relatively large experimental temperature, 800°C. In fact, in our experiments, crystal nucleation cannot precede bubble nucleation because the run temperature is about 50–100°C larger than the liquidus of a rhyolitic liquid with 7 wt% H_2O [14].

3.2. *Critical pressure of homogeneous bubble nucleation*

A fundamental parameter of bubble nucleation dynamics in decompression experiments is the critical pressure of homogeneous nucleation, P_{HoN}, that is, the pressure at which bubbles begin to form by homogeneous nucleation. In the 1000 kPa/s series, homogeneous bubble nucleation did not occur in the experiments quenched at 118.9 or 98.9 MPa (Fig. 3b), whereas all the samples

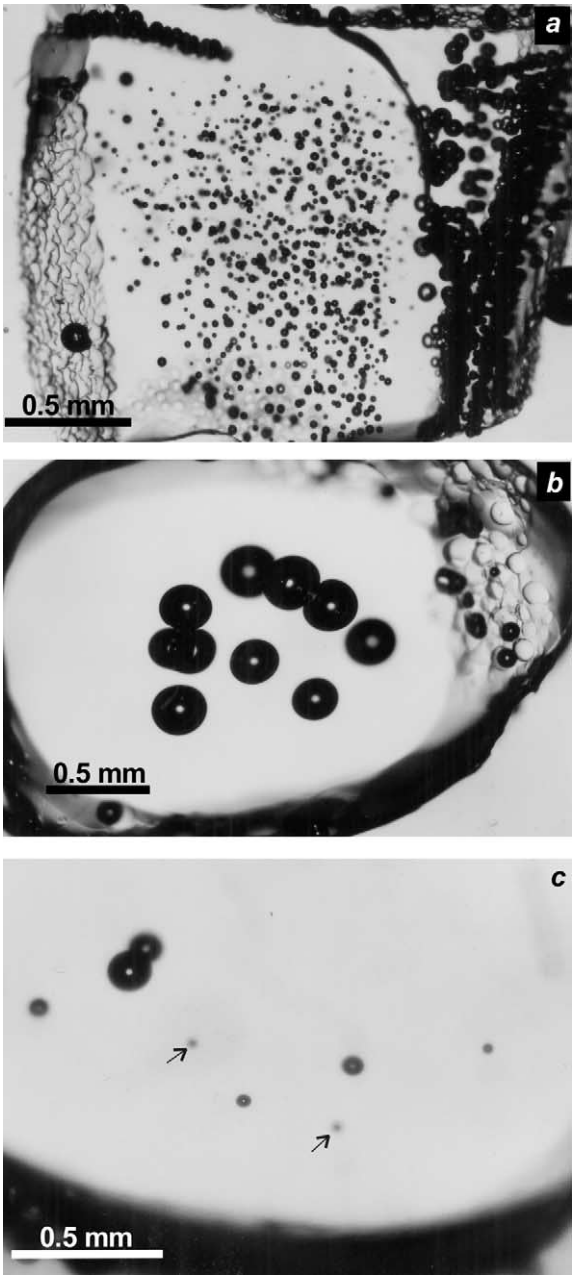

Fig. 4. (a–c) Optical microphotographs of thick sections showing cores of homogeneous bubble nucleation in: (a) sample A2 (1000 kPa/s, $P_f = 79.2$ MPa; note the bubbly fractures in the darker area on the right, and in the upper left corner); (b) sample C8 (27.8 kPa/s, $P_f = 79.5$ MPa); and (c) sample C20 (27.8 kPa/s, $P_f = 88.6$ MPa; the arrows point to two small bubbles out of focus). Comparison of samples A2 and C8 (quenched at the same pressure) shows the major effect of decompression rate on bubble number density and mean bubble size. Scale bars: 500 μm.

quenched at a pressure ≤ 88.4 MPa had a vesiculated core (Figs. 3a, c and 4a). Therefore, P_{HoN} is comprised between 98.9 and 88.4 MPa; in fact, nucleation presumably began at a pressure just slightly larger than 88.4 MPa because the core of sample A5 quenched at 88.4 MPa contained only two bubbles (Table 1). The value of P_{HoN} is bracketed more tightly in the two other experimental series: P_{HoN} is comprised between 84.4 and 90.5 MPa in the 167 kPa/s series, and between 88.6 and 92.1 MPa in the 27.8 kPa/s series (Table 1).

3.3. *Quantitative study of homogeneous nucleation textures*

All the samples quenched at $P_f < 90$ MPa underwent an event of homogeneous bubble nucleation that was responsible for the development of a vesiculated core. The systematic study of core textures revealed two important features (Table 1):

1. For a given sample, the texture of the vesiculated core is homogeneous, showing no spatial variation of bubble number density and mean bubble size. Even when the sample contains two cores separated by a bubbly fracture, both cores have very similar textures (Fig. 3c).
2. The textural parameters show important variations from one experiment to the other: in a given series, they are very sensitive to quench pressure P_f, and at a given value of P_f, they are strongly dependent on decompression rate (compare Fig. 4a and b).

In the 27.8 kPa/s experiments, textural analysis was complicated by the bubbly fractures. The main drawback of the development of bubbly fractures was to reduce the effective sample volume (Fig. 3c). In the absence of bubbly fractures, the sample volume was ≈ 7 mm^3. Depending on the number and location of bubbly fractures, the effective sample volume was reduced to only a few mm^3 in many experiments, and to less than 1 mm^3 in a few ones. In the 1000 and 167 kPa/s series, the textures could still be characterized accurately owing to the large number of bubbles in the cores. On the contrary, in the 27.8 kPa/s series, the reduction of core volumes combined with the much smaller nucleation rates (see below) resulted in very low total numbers of bubbles, from two to 10 (Table 1). With such small numbers of bubbles, it is not possible to locate exactly the boundary of

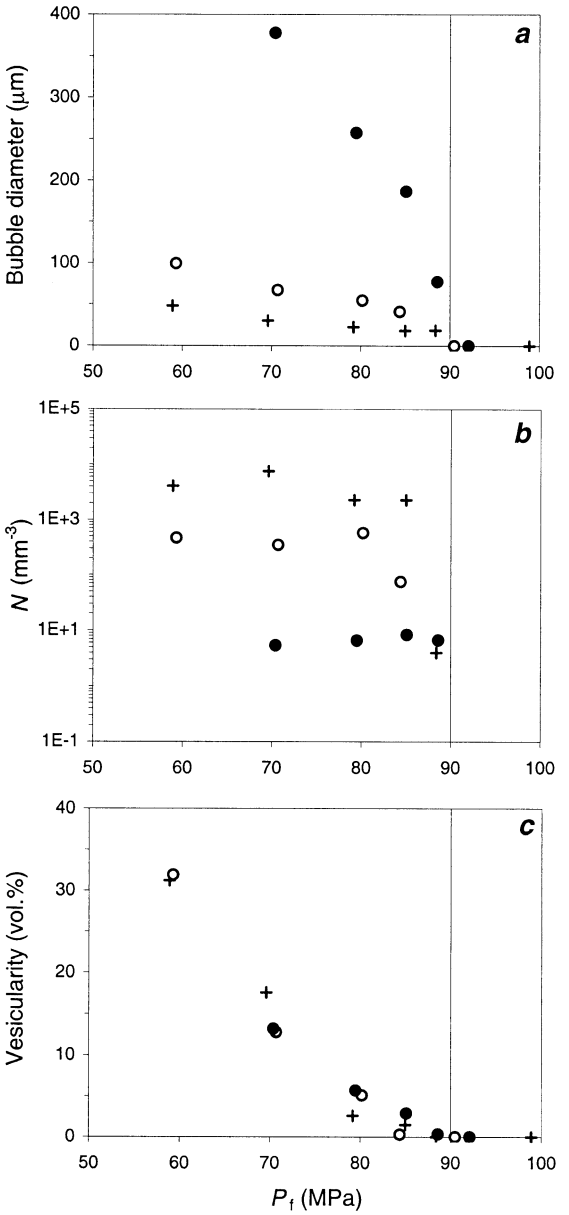

Fig. 5. (a–c) Plots of mean bubble diameter (a), bubble number density (b) and vesicularity (c) as a function of pressure P_f (filled circles: 27.8 kPa/s series; empty circles: 167 kPa/s series; crosses: 1000 kPa/s series). The vertical line at $P_f = 90$ MPa corresponds to the nucleation pressure.

the vesiculated core, and so to measure precisely its volume. Accordingly, the accuracy on bubble number densities and vesicularities in the 27.8 kPa/s series is not better than ±30% (C8, C20) to ±50% (C11, C19).

3.3.1. Bubble sizes

All samples show a unimodal BSD with a moderate dispersion of sizes. An important evolution of BSD and mean bubble size is observed with decreasing pressure (Table 1). At a given decompression rate, the mean bubble size increases with decreasing P_f, and at a given value of P_f, the mean bubble size increases with decreasing decompression rate (Fig. 5a). The evolution of BSD with decreasing pressure is best visible in the 27.8 kPa/s series: sample C20 quenched at 88.6 MPa contains eight bubbles with diameters ranging from 39 to 152 μm (Fig. 4c), whereas the 10 bubbles in sample C8 quenched at 79.5 MPa are nearly equi-sized, with a mean diameter of 258 μm and a standard deviation of 20 μm (Fig. 4b). The large bubbles in sample C20 are presumed to have nucleated early during the decompression experiment (at a pressure equal to P_{HoN}), while the smaller bubbles nucleated just before quenching. Their smaller size cannot be due to bubble–bubble interactions because all bubbles in C20 are far from one another, with distances from center to center of typically 600 μm. The absence of small bubbles in C8 implies that the nucleation event stopped at a pressure lying somewhere between 88.6 and 79.5 MPa.

3.3.2. Bubble number density

The number of bubbles per unit volume of glass, N, increases by about three orders of magnitude with increasing decompression rate: from ≈ 7 mm^{-3} at 27.8 kPa/s to ≈ 6000 mm^{-3} at 1000 kPa/s (Fig. 5b). In the 1000 kPa/s series, N increases strongly from 88.4 to 85.0 MPa and then remains nearly constant from 85.0 to 58.9 MPa (Table 1). To a lesser extent, N shows the same behavior in the 167 kPa/s series; in the 27.8 kPa/s series, N is nearly independent of P_f and equals 7 mm^{-3} (Fig. 5b). The fact that N reached a plateau implies that, at some point along the decompression path, the nucleation rate began to decrease and eventually nucleation stopped.

3.3.3. Vesicularity

With decreasing pressure, vesicularity increased from a few tenths of a percent at $P_f \approx 90$ MPa to 31 vol% at $P_f \approx 60$ MPa (Fig. 5c). Within the range of experimental pressures we did not detect a measurable effect of decompression rate on vesicularity. In particular, samples B23 (167 kPa/s; $P_f = 59.3$ MPa) and A1 (1000 kPa/s; $P_f = 58.9$ MPa) have nearly equal vesicularities: 31.9 and 31.2 vol%, respectively.

3.4. Water contents

At the end of a decompression experiment, the water content in the liquid is assumed to be at a minimum close to the bubbles and to increase with increasing distance from the bubbles. For each sample, five to eight microprobe analyses of the glass were made within the vesiculated core but as far as possible from the bubbles visible in the polished section (even in the most densely nucleated samples, such as A1, it was possible to find large glass pools, 100–200 μm in diameter, convenient for microprobe analysis). The water contents were computed from microprobe analyses using the difference method. This technique has a relatively low precision (>0.5 wt%, mostly due to the difficulty to measure Na abundances in hydrous, SiO_2-rich glasses [24]), but it has an excellent spatial resolution that allowed us to sample a minimal glass volume by using a 10 μm beam size. The water contents measured in two starting glasses with the electron microprobe were within ±0.5 wt% of the FTIR values.

The water contents measured in the glass far from the bubbles provide strong arguments for disequilibrium degassing (Table 1): First, the water contents for P_f in the range 90–70 MPa are close to the initial water content: 6–7 wt%, as compared to equilibrium values of 4–3.4 wt% [21,22]. Second, the water contents in the two experiments at $P_f \approx 59$ MPa (B23 and A1) have decreased to ≈ 5 wt% but are still much larger than the equilibrium value predicted by the solubility

models of Zhang [21] and Tamic et al. [22]: ≈3.2 wt%.

4. Discussion

4.1. Supersaturation pressures required for homogeneous bubble nucleation

Homogeneous nucleation of water bubbles in a rhyolitic liquid with 7 wt% H_2O requires a very large degree of volatile supersaturation. The nucleation pressure in the three experimental series is indeed equal to 90 ± 2 MPa, as compared to a volatile saturation pressure of 240 ± 5 MPa. Accordingly, at 7 wt% H_2O, the difference ΔP_{HoN} between saturation pressure and nucleation pressure is equal to 150 MPa (± 7 MPa).

In the classical theory of bubble nucleation, the critical supersaturation pressure required to produce a nucleation rate equal to J is given by [11,25]:

$$\Delta P_{HoN} = \sqrt{\frac{16\pi\sigma^3}{3kT\ln(J_0/J)}} \quad (1)$$

where ΔP_{HoN} is in Pa, k is the Boltzmann constant ($k = 1.3805\times10^{-23}$ J/K), temperature T is in Kelvin, the nucleation rate J is in m^{-3} s^{-1}, and σ is the surface tension of the bubble–liquid interface (N m^{-1}). Parameter J_0 (in m^{-3} s^{-1}) is given by:

$$J_0 = \frac{2\Omega_L n_0^2 D}{a_0}\sqrt{\frac{\sigma}{kT}} \quad (2)$$

where Ω_L is the volume of water molecules in the liquid ($\Omega_L = 3\times10^{-29}$ m^3), n_0 is the number of water molecules per unit volume of liquid, a_0 is the mean distance between water molecules ($a_0 \approx n_0^{-1/3}$), and D is water diffusivity in the liquid. For a mass fraction of molecular water X_m in the liquid, n_0 is equal to $6.02\times10^{23} X_m \rho_{liq}/m$, where 6.02×10^{23} is the Avogadro number, ρ_{liq} is liquid density (2245 kg/m^3), and m is the molar mass of water (0.018 kg/mol). In rhyolitic liquids with a total H_2O mass fraction $X = 0.07$ (H_2O molecules+OH groups) at 800°C, one has X_m = 0.032 [21] and $D = 1.5\times10^{-11}$ m^2/s (at the pressures where bubble nucleation proceeds: ≈90 MPa [26]).

In the next section, we show that the term σ in Eq. 1 must be set equal to 0.106 (± 0.001) N m^{-1} to account for the values of ΔP_{HoN} observed in our experiments (≈150 MPa). There are only very few measurements of the surface tension of rhyolitic liquids under water pressures [27,28], and none corresponding closely to the physical conditions and chemical composition of our study. However, our estimate of 0.106 N m^{-1} is in quite good agreement with Bagdassarov et al.'s measurements for a haplogranitic liquid [28], which predict a value of 0.087 N m^{-1} in the P–T conditions of our experiments.

4.2. The effect of decompression rate on nucleation pressure

We used Eqs. 1 and 2 to estimate the effect of decompression rate on nucleation pressure and nucleation rate. In the calculations, pressure was decreased from $P_0 = 240$ to 0 MPa by steps ΔP of 1 or 0.1 MPa. At each pressure $P_i = P_0 - i\cdot\Delta P$, where i is an integer ≥0, we computed the supersaturation pressure $\Delta P_i = P_0 - P_i$, the nucleation rate J_i, the time t_i, and the bubble number density N_i. Variables t_i and N_i are given by:

$$t_i = i\cdot\Delta P\cdot|dP/dt|^{-1} \quad (3)$$

$$N_i \approx \sum_{j=1}^{i}\left(\frac{J_{j-1}+J_j}{2}\right)\cdot(t_j - t_{j-1}) \quad (4)$$

where $|dP/dt|$ is the decompression rate. The evolutions of J_i and N_i as a function of pressure are shown in Fig. 6a. Unlike the nucleation rate, the bubble number density is sensitive to decompression rate: at a given pressure (below ≈95 MPa), the smaller the decompression rate, the larger the bubble number density. The explanation is straightforward: with decreasing decompression rate, the average nucleation rate $(J_{i-1}+J_i)/2$ in the pressure interval P_{i-1} to P_i is constant, but the term $(t_i - t_{i-1})$ increases so that the number of bubbles nucleated between P_{i-1} and P_i increases.

Let us compare the experimental and theoreti-

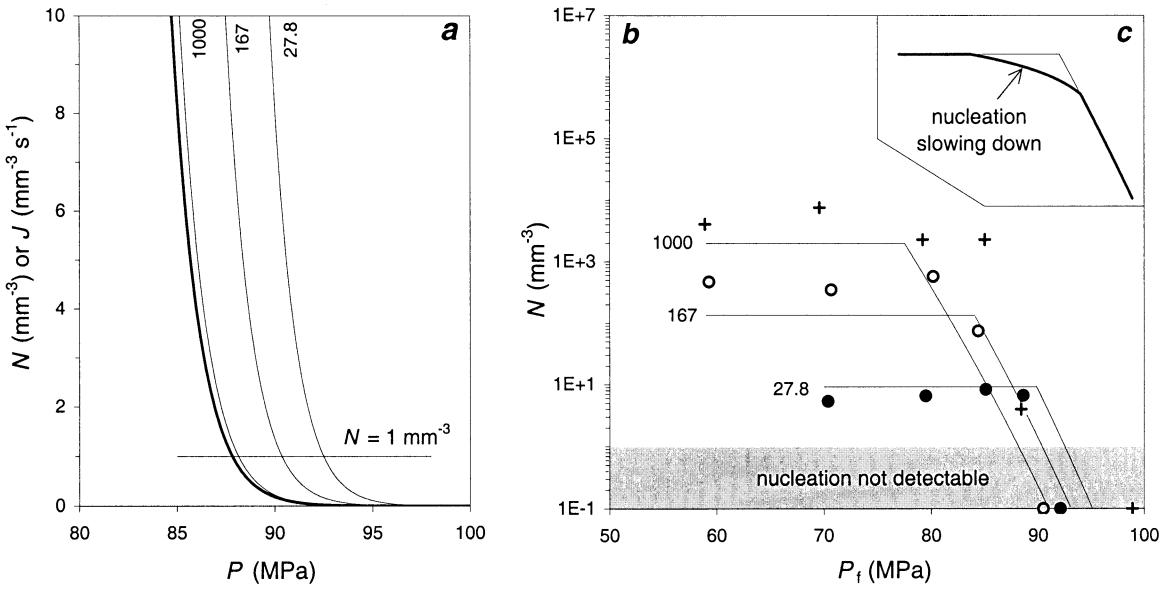

Fig. 6. (a) Evolution of the nucleation rate J (thick line) and of bubble number densities N (thin lines; the labels correspond to the decompression rate: 27.8, 167, and 1000 kPa/s) with decreasing pressure as predicted by the classical theory of nucleation. The calculations were made using Eqs. 1–4, with $X_t = 0.07$ ($X_m = 0.032$) and $\sigma = 0.106$ N m^{-1} (see text for details). (b) Plot of N as a function of P_f comparing the experimental data (solid circles: 27.8 kPa/s; empty circles: 167 kPa/s; crosses: 1000 kPa/s) and composite theoretical trends based on the classical theory of nucleation (on the right, where N increases with decreasing P_f) and on Toramaru's [4] numerical study of vesiculation in an ascending magma (on the left, where N is stationary). The three data points along $N = 0.1$ mm^{-3} correspond to experiments quenched above the nucleation pressure (so strictly at $N = 0$ mm^{-3}). The lower part of the figure is shaded to emphasize the fact that nucleation events leading to densities of 0.1–1 mm^{-3} will probably not be detected in samples of only a few mm^3. (c) Modification (qualitative) of the theoretical trends in (b) to show that nucleation should not stop abruptly but instead slow down due to a progressive decrease of the volume of supersaturated liquid (see text for further explanation).

cal nucleation pressures. To do so, we first have to estimate the minimum number density of bubbles detectable in our experiments. In a sample of volume v, a nucleation event can only be detected if it produces at least one bubble, that is if the number density of bubbles exceeds v^{-1}. Our samples are a few mm^3 in volume, so nucleation becomes detectable when N exceeds ≈ 1 mm^{-3}. With this constraint, surface tension must be set to 0.106 (± 0.001) N m^{-1} to obtain theoretical nucleation pressures in agreement with the experimental ones. Indeed, with $\sigma = 0.106$ N m^{-1}, the pressure at which $N_i \approx 1$ mm^{-3} equals 92.5 MPa at 27.8 kPa/s, 90.4 MPa at 167 kPa/s, and 88.1 MPa at 1000 kPa/s (Fig. 6a). This small effect of decompression rate on nucleation pressure is in good agreement with our observations: in our experiments, P_{HoN} may either be interpreted to be nearly constant and equal to 90 ± 2 MPa or to increase from 89 MPa in the 1000 kPa/s series to 92 MPa in the 27.8 kPa/s series.

4.3. Competition between bubble nucleation and diffusive bubble growth

Our experimental results show that N rapidly ceased to increase with decreasing pressure and reached a stationary value, N_{stat}, equal to 6.8, 470, and 5800 mm^{-3}, at 27.8, 167, and 1000 kPa/s, respectively (Fig. 5b; for each series N_{stat} is calculated by averaging the N values along the plateau in the N vs. P_f diagram). Decompression experiments in the CO_2–H_2O–polymer system [5] also yielded very short nucleation events leading

to stationary bubble number densities. The new finding in our study is that the stationary value of N is strongly sensitive to decompression rate (Fig. 5b). A similar behavior, not predicted by classical theory (Fig. 6a), was described in a numerical study of vesiculation in a magma ascending at constant velocity [4]. In these simulations, the nucleation events were of very short duration: the nucleation rate first increased rapidly, in agreement with classical nucleation theory, but then decreased and finally dropped to zero. Bubble number density reached a maximum value at the end of the nucleation event and was thereafter stationary in time. This behavior was interpreted as a result of a competition between bubble nucleation and diffusive bubble growth [4]. As water diffuses from the liquid to a growing bubble, the degree of supersaturation of the liquid around the bubble decreases. At the beginning of the nucleation event, when the number density of bubbles is small, diffusive bubble growth affects only a small volume fraction of the liquid: everywhere else, water concentration is equal to the initial value, and nucleation can proceed with decompression. With increasing N, the average distance between neighboring bubbles decreases and diffusive bubble growth affects an increasing volume fraction of liquid. Once a critical value of N is attained, diffusive bubble growth can keep pace with decompression: the degree of water supersaturation is everywhere reduced below the critical value required for bubble nucleation and does not increase with decreasing pressure. At this point, the system enters a regime where N is stationary and textural evolution is controlled by the growth of existing bubbles.

For a given value of σ, the final bubble number density, N_{stat}, depends primarily on water diffusiv-

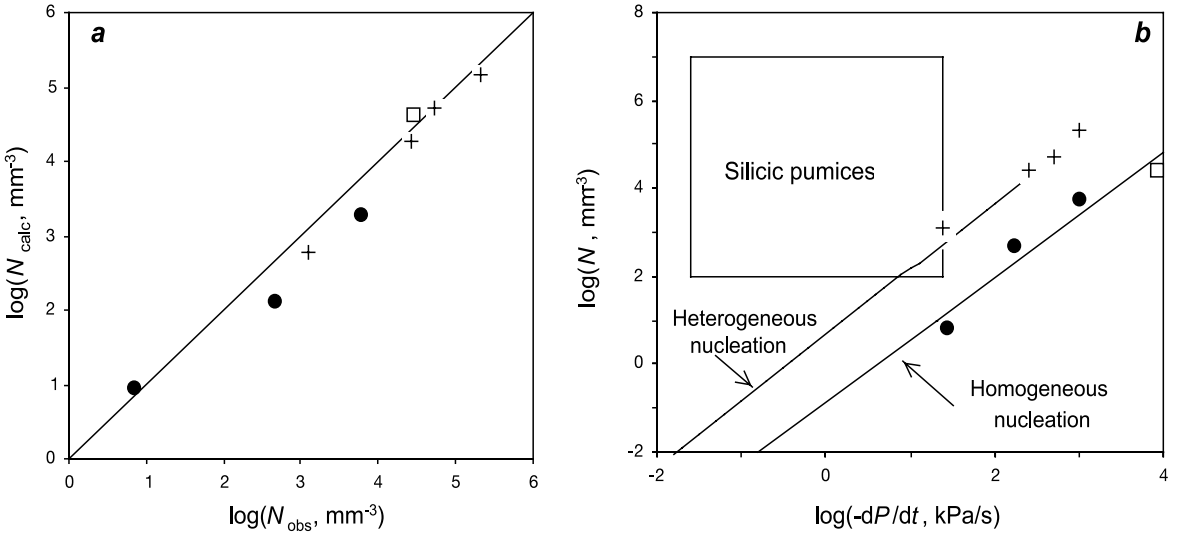

Fig. 7. (a) Comparison of observed and calculated bubble number densities, N_{obs} and N_{calc} (mm^{-3}), respectively: filled circles, this study; empty square, Mangan and Sisson [10]; crosses, Gardner et al. [13]. The relation used to compute N_{calc} is from Toramaru [4]. The following values were used in the calculations (H_2O diffusivities were computed using Zhang and Behrens' [26] model): $C_0 = 5.3\times10^{27}$ m^{-3}, $P_0 = 2.4\times10^8$ Pa, $T = 1073$ K, $\sigma = 0.106$ N m^{-1}, and $D = 1.5\times10^{-11}$ m^2/s for this study; $C_0 = 4.0\times10^{27}$ m^{-3}, $P_0 = 2\times10^8$ Pa, $T = 1173$ K, $\sigma = 0.106$ N m^{-1}, and $D = 1.7\times10^{-11}$ m^2/s for [10]; and $C_0 = 4.4\times10^{27}$ m^{-3}, $P_0 = 2\times10^8$ Pa, $T = 1098$ K, $\sigma = 0.025$ N m^{-1}, and $D = 1.5\times10^{-11}$ m^2/s for [13]. (b) Plot of observed bubble number densities (mm^{-3}) as a function of decompression rate (in kPa/s; same symbols as in (a)). The line labeled 'Homogeneous nucleation' is the best linear fit to the experimental data of this study and [10]. The line labeled 'Heterogeneous nucleation' corresponds to densities computed in the case of a very low effective surface tension: 0.025 N m^{-1} ($C_0 = 4.4\times10^{27}$ m^{-3}, $P_0 = 2\times10^8$ Pa, $T = 1098$ K, and $D = 1.5\times10^{-11}$ m^2/s). The box 'Silicic pumices' shows the typical range of magma ascent rates (from 0.001 to 1 m/s; or decompression rates of 0.025 to 25 kPa/s) and the bubble number densities measured in natural silicic pumices (from 10^2 to 10^7 mm^{-3}).

ity in the liquid and on decompression rate. An approximate relationship between N_{stat} and the main physical parameters is [4]:

$$N_{stat} \approx 10 \cdot C_0 \left(\frac{16\pi\sigma^3}{3kTP_0^2}\right)^{-2} \left(\frac{\Omega_L P_0}{kT}\right)^{-1/4} \left(\frac{kTC_0 D P_0^2}{4\sigma^2 |dP/dt|}\right)^{-3/2} \quad (5)$$

where C_0 is the volatile concentration at the initial saturation pressure P_0 (C_0 is expressed as the number of volatile molecules per unit volume of liquid: 5.3×10^{27} m^{-3} for $X=0.07$). For $P_0=240$ MPa, $T=1073$ K, $\sigma=0.106$ N m^{-1} (as determined from the critical nucleation pressures in our experiments), and $D=1.5\times10^{-11}$ m^2/s (computed using Zhang and Behrens' model [26] for $T=1073$ K and P equal to the nucleation pressure: 90 MPa), Eq. 5 yields $N_{stat}=9.2$, 135, and 1987 mm^{-3} for 27.8, 167, 1000 kPa/s, respectively. Accordingly, without any adjustments of the main physical parameters, the calculated number densities reproduced the experimental ones (6.8, 470, and 5800 mm^{-3}; Fig. 7a) within a factor 0.3–1.4.

4.4. Duration and rate of nucleation

Three stages may be distinguished in the nucleation experiments (Fig. 6c). (1) First, J and N increase rapidly with decreasing pressure (below P_{HoN}), as predicted by the classical theory of nucleation. (2) Then, nucleation slows down because the volume of liquid with a sufficient degree of supersaturation decreases due to water depletion around growing bubbles. (3) Finally, at a pressure P_{end}, the nucleation rate becomes negligible and N reaches a stationary value, N_{stat}, as predicted by [4]. Knowing P_{HoN}, P_{end}, and N_{stat} (6.8, 470, and 5800 mm^{-3} for 27.8, 167, 1000 kPa/s), it is possible to estimate the duration of the nucleation event, Δt, which is the time elapsed between P_{HoN} and P_{end}, and the average nucleation rate, $N_{stat}/\Delta t$. For P_{HoN}, we use the following values: 92 MPa at 27.8 kPa/s, 90 MPa at 167 kPa/s, and 89 MPa at 1000 kPa/s. It is more difficult to estimate precisely P_{end} because we only have four to five data points for each decompression series. We take $P_{end} \approx 75$ MPa at 1000 kPa/s, 80 MPa at 167 kPa/s, and 85 MPa at 27.8 kPa/s (Fig. 5b). The estimate of P_{end} at 27.8 kPa/s is based on the BSDs of samples C20 and C8, which show that the nucleation event ended between 88.6 and 79.5 MPa (Fig. 4b,c). With increasing decompression rate, the duration of the nucleation event decreased and the average nucleation rate increased: $\approx$250 s and 0.03 mm^{-3} s^{-1} at 27.8 kPa/s; $\approx$60 s and 8 mm^{-3} s^{-1} at 167 kPa/s; and $\approx$14 s and 400 mm^{-3} s^{-1} at 1000 kPa/s.

In a system with N_{stat} bubbles/m^3, the mean half distance between bubbles is $L_{B-B} \approx (3/[4\pi N_{stat}])^{1/3}$ [6,29], that is, 330, 80, and 35 μm at 27.8, 167, and 1000 kPa/s, respectively. To explain the stopping of nucleation, the length scale of water diffusion for a time scale Δt must be nearly equal to L_{B-B}. In three dimensions, the distance traveled by diffusion is $L_D \approx (6D\Delta t)^{1/2}$ [30] so that the water-depleted halo around a growing bubble is expected to have a width comprised between $2\sqrt{D\Delta t}$ and $3\sqrt{D\Delta t}$. For $D=1.5\times10^{-11}$ m^2/s, $L_D \approx 150$, 73, and 35 μm at 27.8, 167, and 1000 kPa/s, respectively. The excellent agreement between L_{B-B} and L_D at 167 and 1000 kPa/s supports the interpretation that nucleation stopped due to the competitive effect of diffusive bubble growth. The very small nucleation rates in the 27.8 kPa/s series combined with our small sample volumes may have resulted in a premature stopping of nucleation, explaining the poor agreement between L_{B-B} and L_D. By premature stopping, we mean that N stopped to increase measurably although J was still not null, leading to an underestimation of N_{stat}, Δt and L_D, and an overestimation of L_{B-B}.

4.5. Comparison with previous experimental work

The effect of ascent rate on degassing of rhyolitic magmas was studied experimentally by Gardner et al. [13] and Mangan and Sisson [10]. Mangan and Sisson studied homogeneous bubble nucleation in a rhyolitic liquid saturated with water at 200 MPa and 900°C ($X=0.052$), and decompressed at 8500 kPa/s (they also made experiments at slower decompression rates but these experiments suffered water losses). Homogeneous bubble nucleation in their system required super-

saturation pressures of 150 MPa, as in our system. In their series at 8500 kPa/s, N first increased and then seemed to stabilize at a value of $\approx 28\times10^3$ bubbles/mm^3. This value plots well on our trend of increasing N with increasing decompression rate (Fig. 7b), and is in reasonably good agreement with the density computed using Eq. 5: 44×10^3 mm^{-3} (Fig. 7a).

In Gardner et al.'s [13] work, bubble nucleation was heterogeneous and required very low supersaturation pressures: ≤ 20 MPa. Despite this major difference with our system, there are two results that are directly comparable to ours. First, at a given decompression rate, N was nearly stationary (or even decreased slightly with decreasing pressure, presumably due to bubble coalescence). Second, N was strongly sensitive to decompression rate: it increased from 1.5×10^3 mm^{-3} at 25 kPa/s, to 29×10^3 mm^{-3} at 250 kPa/s, to 55×10^3 mm^{-3} at 500 kPa/s, and to 216×10^3 mm^{-3} at 1000 kPa/s (Fig. 7b). The relatively large value of N at 25 kPa/s (it is 100 times larger than in our 27.8 kPa/s series) was sufficient to allow equilibrium degassing [13].

4.6. Volcanological implications

The results of our experimental study may be summarized as follows:

1. The degree of supersaturation required for homogeneous bubble nucleation in the rhyolite–H_2O system is very large ($\Delta P_{HoN} \approx 150$ MPa for 7.0 wt% water content), in keeping with former studies [8–10]. In addition, our experiments demonstrate that ΔP_{HoN} is almost independent of decompression rate: nucleation pressure decreased by ≤ 3 MPa for a 36-fold increase in decompression rate.
2. Our major experimental finding is that, after a short nucleation event leading to a unimodal BSD (Figs. 3, 4), nucleation stopped and the bubble number density N reached a stationary value that was strongly sensitive to decompression rate: the smaller the decompression rate, the smaller the bubble number density (Fig. 5b). At low decompression rate, the smaller value of N was compensated by a larger mean bubble size, so that, at a given pressure, vesicularity was almost independent of decompression rate (Fig. 5a,c).
3. The nucleation behavior in our experiments is qualitatively and quantitatively similar to the behavior described in a numerical simulation of vesiculation in an ascending magma [4]. It is dictated by a competition between bubble nucleation and diffusive bubble growth, which depletes in water the surrounding liquid and therefore reduces the degree of volatile supersaturation. Once a critical value of N is attained, diffusive bubble growth can keep pace with decompression and prevent the degree of volatile supersaturation in the liquid to increase with decreasing pressure.

In the following, we discuss the volcanological implications of our results for the rhyolite–H_2O system. Applications to other systems may not be warranted: for instance, our study in the rhyolite–H_2O–CO_2 system [9] suggested that CO_2 has an important effect on both ΔP_{HoN} and N.

4.6.1. Implications for bubble number densities in silicic magmas

If we extrapolate the experimental data for homogeneous bubble nucleation to the typical ascent rates of silicic magmas (0.001 to 1 m/s, that is, decompression rates of ≈ 0.025 to 25 kPa/s [17]; these conversions only apply in the deep conduit where the pressure gradient is hydrostatic, not close to the fragmentation level), we obtain densities of 7×10^{-4} to 10 bubbles/mm^3 (Fig. 7b). Bubble number densities produced by heterogeneous nucleation are larger than those produced by homogeneous nucleation, but, for slow ascent rates, they should rarely exceed 10^3 mm^{-3}, as argued in the next section. Most of these estimates are orders of magnitude lower than the densities measured in natural silicic pumices: 10^2–10^7 mm^{-3} [31–34].

The huge densities in silicic pumices are due to the presence of a multitude of small bubbles, 10–100 μm in diameter. In addition to these small bubbles, silicic pumices usually contain a population of large bubbles, a few hundreds of microns to a few millimeter in diameter [31–36]. Although the total volume of large bubbles is quite elevated (they make 10–40% of the bulk vesicularity), their

number densities are relatively small: 0.1–100 mm^{-3} (as computed from vesicle volume distributions in [33,34], using simple stereological approximations). Classically, only one nucleation event is assumed during magma ascent [13,36]: the large bubbles are interpreted either as pre-eruptive bubbles nucleated in a magma chamber [13,31] or as resulting from the coalescence of small bubbles [33–35]. The fact that the number densities of large bubbles in natural pumices are in good agreement with the values of N expected at low decompression rates (Fig. 7b) suggests to us that a third possibility should be explored in the future: both the small and the large bubbles could be syn-eruptive and correspond to two successive nucleation events in the volcanic conduit. The first event would occur relatively deep in the conduit and yield a moderate number of bubbles (10^{-2} to 10^{2} mm^{-3}, depending on ascent rate, nucleation mechanism, etc.) that will have time to grow to final sizes of a few hundreds of micrometers to a few millimeters. The second event would yield a very large number of small bubbles and could be related to the dramatic increase of decompression rate that precedes fragmentation [37,38] and/or to extensive microlite crystallization that would allow bubble nucleation at a supersaturation pressure significantly lower than in the case of homogeneous nucleation [11]. Only the first nucleation event is documented in our experiments, but theoretical studies of bubble nucleation and growth in an ascending magma suggested that a second nucleation event could occur at a shallow level in the conduit [6,39].

4.6.2. *Implications for the kinetics of heterogeneous bubble nucleation*

A reappraisal of Gardner et al.'s [13] study suggests that the number density of bubbles in the case of heterogeneous nucleation is not controlled by the number of potential nucleation sites (for instance, the number of phenocrysts), but rather that it is firstly controlled by the decompression rate, H_2O diffusivity and the critical supersaturation pressure, as in the case of homogeneous nucleation. This conclusion is based on two arguments. (1) In their decompression experiments, N decreased with decreasing decompression rate (Fig. 7b). (2) Their observed densities are well reproduced by Eq. 5, provided that an effective value of 0.025 N m^{-1} is taken for surface tension to account for bubble nucleation at a supersaturation pressure ≤ 20 MPa (Fig. 7a; the 'effective surface tension' is equivalent to σ times $\phi^{1/3}$, where ϕ is a function of the wetting angle of bubbles on crystal faces [11]). Accordingly, the final bubble number density appears to be dictated by a competition between bubble nucleation and diffusive bubble growth, whether or not crystals are present (however, if the number density of phenocrysts is smaller than the value of N predicted by Eq. 5, the number of phenocrysts might become the limiting factor and control the bubble number density). The main difference between the two types of bubble nucleation is that heterogeneous nucleation requires a much lower critical supersaturation pressure, ΔP_N, than homogeneous nucleation: down to 5 MPa in the presence of Fe–Ti oxides [6,11]. At given decompression rate and water diffusivity, N increases with decreasing ΔP_N: for $\Delta P_N \approx 20$ MPa ($\sigma\phi^{1/3} \approx 0.025$ N m^{-1}), N ranges from 0.02 mm^{-3} at 0.025 kPa/s to 600 mm^{-3} at 25 kPa/s (Fig. 7b); for $\Delta P_N \approx 5$ MPa ($\sigma\phi^{1/3} \approx 0.010$ N m^{-1}), N ranges from 0.3 mm^{-3} at 0.025 kPa/s to 9000 mm^{-3} at 25 kPa/s. These calculations suggest that, even in the case of heterogeneous bubble nucleation, bubble number densities in magmas ascending at velocities of 0.001–1 m/s may be much smaller than densities observed in most natural silicic pumices.

4.6.3. *Equilibrium vs. non-equilibrium degassing*

Our study provides the following constraints on the kinetics of degassing:

1. The intuitive idea that a slow magma ascent should result in near-equilibrium degassing may not be valid because a smaller ascent rate yields a smaller number density of bubbles. For instance, the two experiments at $P_f \approx 59$ MPa have similar degrees of water saturation (as indicated by similar vesicularities and final water contents; Table 1) despite a factor 6 difference in decompression rate. More experiments at low pressures will be necessary to establish whether or not the larger value of N at high decompression rates is suf-

ficient to fully compensate the reduced time scale for diffusive bubble growth.

2. A strong departure from equilibrium must be the rule in the case of homogeneous bubble nucleation because, in the absence of crystals, a rhyolitic liquid can sustain very large degree of water supersaturation without nucleating bubbles. First, the nucleation event will be strongly delayed: by 150 MPa in the present experiments (see also [8–10]). Second, homogeneous nucleation will yield a relatively small bubble number density (Fig. 7b), sufficient to reduce everywhere the degree of supersaturation pressure below the critical value for nucleation, but presumably not sufficient to ensure near-equilibrium degassing.
3. In the presence of a large number of favorable substrates (such as Fe–Ti oxides [11]), heterogeneous nucleation can give rise to a relatively large number density of bubbles at a pressure close to the saturation pressure so that degassing may proceed under near-equilibrium conditions. The question is whether or not such substrates exist with number densities sufficient to really dominate the nucleation process [10].

4.6.4. Future developments

Our experimental results are in good agreement with theoretical predictions (Fig. 6b). First, assuming a rhyolite–H_2O surface tension of 0.106 N m^{-1}, the classical theory of nucleation provides a good description of the initial stages of nucleation in the experiments. Second, the rapid arrest of nucleation and the strong effect of decompression rate on bubble number density observed in the experiments are in qualitative and quantitative agreement with numerical simulations of vesiculation in ascending magmas [4]. The good agreement between theory and experiments is very promising and suggests that vesiculation models including properly the kinetics of bubble nucleation could be running in the near future. At present, however, the development of such models is hampered by the poor knowledge of the supersaturation pressures required for bubble nucleation. Systematic decompression experiments are required to determine this parameter over the range of chemical and physical conditions prevailing in natural systems (presence of CO_2, Cl in addition to H_2O, silicate liquids of intermediate compositions, phenocryst-bearing magmas, etc.).

Acknowledgements

This research program was supported by the Institut National des Sciences de l'Univers (Equipement Mi-Lourds 1997 and Programme National des Risques Naturels). It benefited from discussions with Ariel Provost, Hélène Massol, Tim Druitt, Daniel Vielzeuf, Pierre Boivin, and Régis Thiéry. Christian de Jonghe was involved in the preliminary stages of this study and we thank him for his contribution; the P–T path in Fig. 1 is from his Master's thesis (Clermont-Ferrand, 2001). Special thanks are due to the following persons: Philippe Cacault for technical assistance with the operation of the automatic decompression system; Jean-Michel Beny and Michel Pichavant for their help with the FTIR analyses; Michèle Veschambre and Jean-Luc Devidal for technical assistance with the electron microprobe. The manuscript was improved by the constructive reviews of Jim Gardner, Oded Navon, Youxue Zhang, and Don Dingwell. Contribution INSU-CNRS no. 353.*[BW]*

References

[1] J. Verhoogen, Mechanics of ash formation, Am. J. Sci. 249 (1951) 729–739.
[2] A. Toramaru, Vesiculation process and bubble size distributions in ascending magmas with constant velocities, J. Geophys. Res. 94 (1989) 17523–17542.
[3] R.S.J. Sparks. J. Barclay, C. Jaupart, H.M. Mader, J.C. Phillips, Physical aspects of magma degassing I. Experimental and theoretical constraints on vesiculation, in: M.R. Carroll, J.R. Holloway (Eds.), Volatiles in Magmas, Rev. Mineral. 30 (1994) 413–445.
[4] A. Toramaru, Numerical study of nucleation and growth of bubbles in viscous magmas, J. Geophys. Res. 100 (1995) 1913–1931.
[5] Y. Zhang, B. Sturtevant, E.M. Stolper, Dynamics of gas-driven eruptions: experimental simulations using CO_2–H_2O–polymer system, J. Geophys. Res. 102 (1997) 3077–3096.
[6] O. Navon, V. Lyakhovsky, Vesiculation processes in silicic magmas, in: J.S. Gilbert, R.S.J. Sparks (Eds.), The

Physics of Explosive Volcanic Eruptions, Geol. Soc. London Spec. Publ. 145, 1998, pp. 27–50.
[7] R.S.J. Sparks, The dynamics of bubble formation and growth in magmas: a review and analysis, J. Volcanol. Geotherm. Res. 3 (1978) 1–37.
[8] C.C. Mourtada-Bonnefoi, D. Laporte, Experimental study of homogeneous bubble nucleation in rhyolitic magmas, Geophys. Res. Lett. 26 (1999) 3505–3508.
[9] C.C. Mourtada-Bonnefoi, D. Laporte, Homogeneous bubble nucleation in rhyolitic magmas: an experimental study of the effect of H_2O and CO_2, J. Geophys. Res. 107 (2002) 10.1029/2001JB000290.
[10] M. Mangan, T. Sisson, Delayed, disequilibrium degassing in rhyolite magma: decompression experiments and implications for explosive volcanism, Earth Planet. Sci. Lett. 183 (2000) 441–455.
[11] S. Hurwitz, O. Navon, Bubble nucleation in rhyolitic melts: Experiments at high pressure, temperature and water content, Earth Planet. Sci. Lett. 122 (1994) 267–280.
[12] H.R. Westrich, J.C. Eichelberger, Gas transport and bubble collapse in rhyolitic magma: an experimental approach, Bull. Volcanol. 56 (1994) 447–458.
[13] J.E. Gardner, M. Hilton, M.R. Carroll, Experimental constraints on degassing of magma: isothermal bubble growth during continuous decompression from high pressure, Earth Planet. Sci. Lett. 168 (1999) 201–218.
[14] A.G. Simakin, P. Armienti, M.B. Epel'baum, Coupled degassing and crystallisation experimental study at continuous pressure drop, with application to volcanic bombs, Bull. Volcanol. 61 (1999) 275–287.
[15] C. Martel, B.C. Schmidt, Decompression experiments as an insight into ascent rates of silicic magmas, Contrib. Mineral. Petrol. 144 (2003) 397–415.
[16] D. Laporte, C. Mourtada-Bonnefoi, Ph. Cacault, Homogeneous bubble nucleation in a rhyolitic liquid: the effect of magma ascent rate, J. Conf. Abstr. 5 (2000) 62.
[17] M.J. Rutherford, J.E. Gardner, Rates of magma ascent, in: H.S. Sigurdsson (Ed.), Encyclopedia of Volcanoes, Academic Press, San Diego, CA, 2000, pp. 207–218.
[18] S. Newman, E.M. Stolper, S. Epstein, Measurement of water in rhyolitic glasses: Calibration of an infrared spectroscopic technique, Am. Mineral. 71 (1986) 1527–1541.
[19] R.A. Lange, I.S.E. Carmichael, Densities of Na_2O–K_2O–CaO–MgO–FeO–Fe_2O_3–Al_2O_3–TiO_2–SiO_2 liquids: New measurements and derived partial molar properties, Geochim. Cosmochim. Acta 51 (1987) 2931–2946.
[20] L.A. Silver, P.D. Ihinger, E. Stolper, The influence of bulk composition on the speciation of water in silicate glasses, Contrib. Mineral. Petrol. 104 (1990) 142–162.
[21] Y. Zhang, H_2O in rhyolitic glasses and melts: measurement, speciation, solubility, and diffusion, Rev. Geophys. 37 (1999) 493–516.
[22] N. Tamic, H. Behrens, F. Holtz, The solubility of H_2O and CO_2 in rhyolitic melts in equilibrium with a mixed CO_2–H_2O fluid phase, Chem. Geol. 174 (2001) 333–347.
[23] S.A. Saltykov, The determination of size distribution of particles in an opaque material from the measurement of the size distribution of their sections, in: H. Helias (Ed.), Stereology, Springer, New York, 1967, p. 163.
[24] J.D. Devine, J.E. Gardner, H.P. Brack, G.D. Layne, M.J. Rutherford, Comparison of microanalytical methods for estimating H_2O contents of silicic volcanic glasses, Am. Mineral. 80 (1995) 319–328.
[25] J.P. Hirth, G.M. Pound, G.R. StPierre, Bubble nucleation, Met. Trans. 1 (1970) 939–945.
[26] Y. Zhang, H. Behrens, H_2O diffusion in rhyolitic melts and glasses, Chem. Geol. 169 (2000) 243–262.
[27] M.B. Epel'baum, I.V. Babashov, T.P. Salova, Surface tension of felsic magmatic melts at high temperatures and pressures, Geochem. Int. 10 (1973) 343–345.
[28] N. Bagdassarov, A. Dorfman, D.B. Dingwell, Effect of alkalis, phosphorus and water on the surface tension of haplogranite melt, Am. Mineral. 85 (2000) 33–40.
[29] A.A. Proussevitch, D.L. Sahagian, A.T. Anderson, Dynamics of diffusive bubble growth in magmas: Isothermal case, J. Geophys. Res. 98 (1993) 22283–22307.
[30] A.C. Lasaga, Kinetic Theory in the Earth Sciences, Princeton University Press, Princeton, NJ, 1998, 811 pp.
[31] A.G. Whitham, R.S.J. Sparks, Pumice, Bull. Volcanol. 48 (1986) 209–223.
[32] A. Toramaru, Measurement of bubble size distributions in vesiculated rocks with implications for quantitative estimation of eruption processes, J. Volcanol. Geotherm. Res. 43 (1990) 71–90.
[33] C. Klug, K.V. Cashman, Vesiculation of May 18, 1980, Mount St Helens magma, Geology 22 (1994) 468–472.
[34] C. Klug, K.V. Cashman, C.R. Bacon, Structure and physical characteristics of pumice from the climatic eruption of Mount Mazama (Crater Lake), Oregon, Bull. Volcanol. 64 (2002) 486–501.
[35] G. Orsi, G. Gallo, G. Heiken, K. Wohletz, E. Yu, G. Bonani, A comprehensive study of pumice formation and dispersal: the Cretaio tephra of Ischia (Italy), J. Volcanol. Geotherm. Res. 53 (1992) 329–354.
[36] K.V. Cashman, M.T. Mangan, Physical aspects of magmatic degassing II. Constraints on vesiculation processes from textural studies of eruptive products, in: M.R. Carroll, J.R. Holloway (Eds.), Volatiles in Magmas, Rev. Mineral. 30 (1994) 447–478.
[37] D.B. Dingwell, Volcanic dilemma: flow or blow?, Science 273 (1996) 1054–1055.
[38] C. Jaupart, Physical models of volcanic eruptions, Chem. Geol. 128 (1996) 217–227.
[39] H. Massol, T. Koyaguchi, Explosive eruption dynamics: coupled effects of vesiculation kinetics and magma ascent, EOS Trans. AGU 82 (2001) Fall Meet. Suppl., Abstr. V21B-0973.